electronics
MDPI

Article

Analysis of Control Strategy of Arc Plasma Power Supply Inverter Module

Yue Li [1], Hailong Yu [1], Chuan Jiang [1,2] and Yong Jin [1,*]

[1] School of Petroleum and Natural Gas Engineering, School of Energy, Changzhou University, Changzhou 213164, China; s21040858002@smail.cczu.edu.cn (Y.L.); yhl@cczu.edu.cn (H.Y.); jiang.chuan@cczu.edu.cn (C.J.)
[2] Jiangsu Provincial Key Laboratory of Solar Energy Science and Technology, Southeast University, Nanjing 210096, China
* Correspondence: kingdeyu@cczu.edu.cn

Abstract: The inverter module serves as a critical component in the conversion of electrical energy within arc plasma power sources, exerting a profound influence on the overall performance and stability of the power supply. Consequently, the meticulous design and precise control of the inverter module are of paramount importance in ensuring the effective operation and application of arc plasma power sources. This paper introduces a dual-closed-loop control system, integrating a voltage outer loop with a current inner loop, as the cornerstone of its inverter module design. It also undertook a comprehensive comparative analysis of various voltage-control strategies, encompassing four control methods (PI, PID, PR, QPR) and two modulation techniques (bipolar modulation and unipolar, carrier-based modulation) under diverse operating conditions. Additionally, simulation experiments were conducted on a prototype 10 kW inverter module using the Matlab/Simulink simulation platform, with evaluation criteria including waveform tracking performance, voltage waveform distortion rate, and steady-state error. The results indicate that in low-frequency operating conditions, the voltage-control strategy employing QPR control plus unipolar, carrier-based modulation, and in high-frequency operating conditions, the voltage-control strategy utilizing PI control plus unipolar, carrier-based modulation exhibited superior waveform tracking performance. The waveform distortion rates were measured at below 0.47% and 4.2%, respectively, aligning perfectly with the stringent standards of IEEE 519. This research provides valuable theoretical support and practical guidance for future engineering endeavors in the field of inverters.

Keywords: arc plasma power supply; Inverter module; PI control; QPR control; unipolar frequency multiplication modulation

Citation: Li, Y.; Yu, H.; Jiang, C.; Jin, Y. Analysis of Control Strategy of Arc Plasma Power Supply Inverter Module. *Electronics* **2023**, *12*, 4400. https://doi.org/10.3390/electronics12214400

Academic Editor: Davide Astolfi

Received: 20 September 2023
Revised: 19 October 2023
Accepted: 22 October 2023
Published: 25 October 2023

1. Introduction

Plasma clean technology is currently at the forefront of international advanced environmental technology. Arc plasma [1,2] is extensively utilized in the disposal of various types of solid waste, due to its high current density, concentrated energy, and high gas enthalpy. This technology shows great potential in the field of environmental management, with promising market prospects. The rapid development of plasma technology [3] has led to a continuous renewal of arc plasma power supplies. The arc plasma power supply [4] plays a crucial role in ensuring the stability of the arc by generating a stable, high-frequency, high-voltage direct current. It comprises several modules, including a rectifier filter module, an inverter module, a high-frequency voltage converter module, and a fast rectifier module. Among these, the inverter module is a critical device, converting direct current into alternating current. During the process of tracking rated voltage and frequency signals, the impact of sudden, high-impact loads can introduce stability errors and system disturbances. Therefore, it is necessary to incorporate voltage and current control strategies within the inverter module to ensure that the system output maintains low harmonic content, thus preserving its performance, stability, and reliability.

Over the course of several decades, the control technology for inverter modules has seen significant development. Scholars from both domestic and international backgrounds have put forth various control methods. Based on the system-modeling approach or mathematical-description methods, inverter control technology can be broadly classified into two main categories: nonlinear control techniques and linear control techniques [5]. Several high performances of nonlinear control schemes, such as deadbeat control [6,7], hysteresis control, predictive control [7,8], iterative learning control [9], and sliding mode control have been implemented for inverters [10,11].

Among these control techniques, the deadbeat control technique, which belongs to the family of predictive regulators, is the most commonly used control technique in several recent applications [12]. When the deadbeat controller is optimally tuned, it offers a faster transient response with a minimal tracking error within a finite number of sampling steps. However, deadbeat control is more susceptible to uncertainties, data mismatches, and noise at higher sampling frequencies.

The hysteresis control method can be employed in a voltage-source inverter to compare the output utility current to the input reference current, thereby generating switching signals for the inverters. Hysteresis control offers several advantages, including simplicity, independence from load factors, and excellent transient response [7,13].

The predictive control method is renowned for its effectiveness in nonlinear control systems. This technique can achieve precise current control with low total harmonic distortion (THD) and noise. However, it is often considered challenging to implement in practical application [14,15].

On the other hand, the sliding mode (SM) control technique has garnered increased interest for both nonlinear and linear loads [16–18]. SM control is widely recognized as the preferred algorithm for implementing an inverter system, due to its exceptional performance. Currently, SM control has gained widespread adoption for its ability to accurately track the AC output of the system [19–22]. However, this control technique, while reducing harmonic levels in the output, has limited capability to reject high-order harmonics. Continuous-time SM control techniques have been proposed in [23,24], where the output filter current is used as a state variable. Nevertheless, the SM control technique, which employs variable switching signals, can lead to an undesirable chattering phenomenon. Hysteresis-based switching has been considered for each leg of the inverter, resulting in increased hardware complexity [25].

Inverter systems, being highly nonlinear in nature, utilize linear control techniques to linearize their models. This approach is straightforward, easy to grasp, and benefits from well-established parameter-tuning methods, making it the most commonly employed control method today. The implementation of linear control enables inverters to demonstrate outstanding steady-state performance and satisfactory dynamic performance. At present, the linear control methods for inverters mainly encompass proportional-integral (PI) control [26], proportional-integral-derivative (PID) control, proportional-resonant (PR) control, quasi-proportional-resonant (QPR) control [27,28], and more. M. Parvez and colleagues [29] conducted a simulation experiment to analyze the application of PI and PR control in single-phase UPS inverters. They compared the performance of these two control approaches in terms of steady-state response, current harmonic levels, and more. Li Jianlin and his team [30] conducted a comparative analysis between two control strategies, PI control and QPR control. They utilized a Matlab simulation model to create two distinct operational scenarios, and compared the external output characteristics of the Power Conversion System (PCS) under these different control conditions. Wang Xiuyun and her team [31] conducted a comparative analysis of three controllers: PI control, PR control, and QPR control. They examined the Bode plots of these controllers, considering their frequency characteristics, gains, and bandwidths to make an informed choice of controller. To validate their decision, they conducted simulation experiments and compared the waveform distortion rates.

The aforementioned studies only compared two or three control methods under a single operating condition. Building on this foundation, our study enhances the control structure of the inverter module by introducing a dual-closed-loop control strategy, incorporating a voltage outer loop and a current inner loop. This innovation leads to improved control precision. Furthermore, we explore various operating conditions to assess the strengths and weaknesses of the four control methods—PI, PID, PR, and QPR—along with the two modulation techniques, bipolar modulation and single-pole, double-frequency modulation. Utilizing the Matlab/Simulink simulation platform, our research conducted simulation experiments on a 10 kW inverter module prototype. We compared and validated these control strategies based on key performance indicators, including waveform tracking accuracy, voltage waveform distortion rates, and steady-state errors. This study seeks to offer both theoretical support and practical guidance for inverter-related projects across diverse operating scenarios.

2. Arc Plasma Power Supply Main Circuit

Figure 1 shows the main circuit of the arc plasma power supply. It comprised a rectifier filter circuit, a full-bridge inverter circuit, a high-frequency transformer, and a fast rectifier circuit. This configuration facilitated the transfer of energy between AC and DC power through an AC-DC-AC-DC conversion process. The rectifier circuit used the unidirectional conductivity of four diodes D1–D4 to rectify the 220 V AC voltage into a single-phase pulsating voltage. The filter circuit used an LC filter circuit, which was double-filtered to obtain a smooth DC voltage. In the inverter circuit, the 50 Hz DC voltage generated by the LC rectifier filter circuit was inverted to produce a 20 kHz AC signal. After passing through the high-frequency transformer and the fast rectifier circuit, a stable 600 V DC signal is generated.

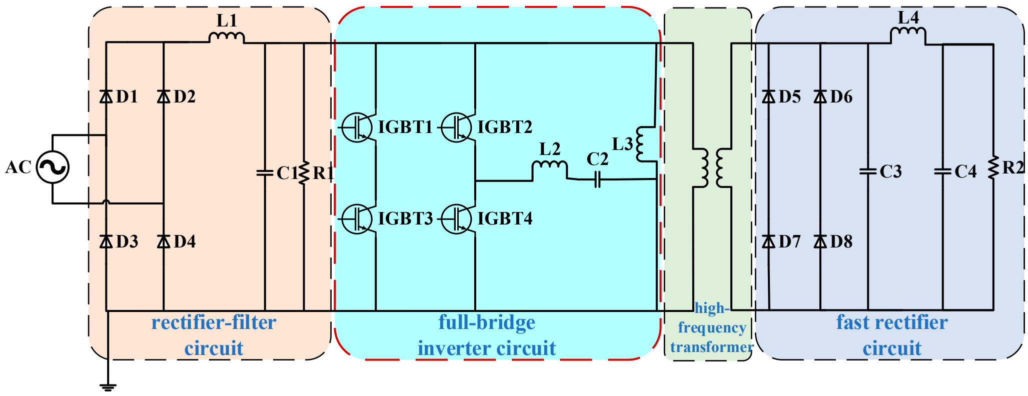

Figure 1. Main circuit of the arc plasma power supply.

An arc plasma power supply with a rated output power of 10 kW was utilized as the subject of simulation experiments. The comprehensive performance of the parameters is presented in Table 1.

Table 1. General Parameters of Arc Plasma Power Supply.

Parameters	Numerical Values	Unit
AC input power	220	V
Power rating	10	kW
Rated input frequency	20	kHz
Total harmonic distortion of the output voltage (THD)	$\leq$5%	/
Output voltage variation	$\pm$3%	/

A study was conducted on the inverter module (the dashed part in Figure 1). The front end of the inverter circuit was replaced by a constant voltage source V_{dc} to simplify the model. After full-bridge inversion, the magnitude of the output voltage was U_d. The main topology structures of single-phase inverter modules are divided into two types: half-bridge and full-bridge. The half-bridge circuit features a simple structure, requiring only a few devices. It generates an output AC voltage amplitude of $U_d/2$. Two capacitors in series are used on the DC side to ensure voltage balance between the two sides. This configuration is well-suited for low-power inverter power supplies. The full-bridge circuit consists of four bridge arms. It produces output voltage and current waveforms with the same shape as the half-bridge circuit. However, the amplitude of the waveforms is twice as high (the magnitude is U_d), making it suitable for high-power applications. IGBT switches (Q1–Q4) were selected for the switching devices. During operation, two control signals were applied to control the switching of Q1 and Q4, as well as of Q2 and Q3. The equivalent topology circuit of the inverter module [32,33] is shown in Figure 2.

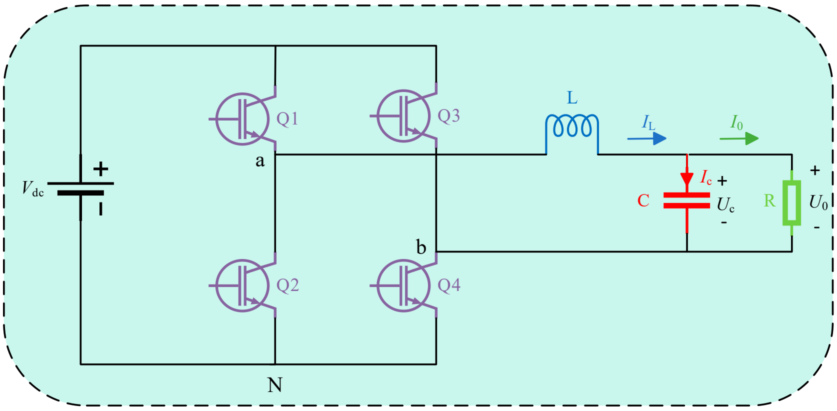

Figure 2. Circuit diagram of the inverter module.

A dual-closed-loop control of voltage and current [34] was adopted to achieve effective control over the topology circuit of the inverter module of the arc plasma power supply. The control block diagram of the inverter module system is shown in Figure 3.

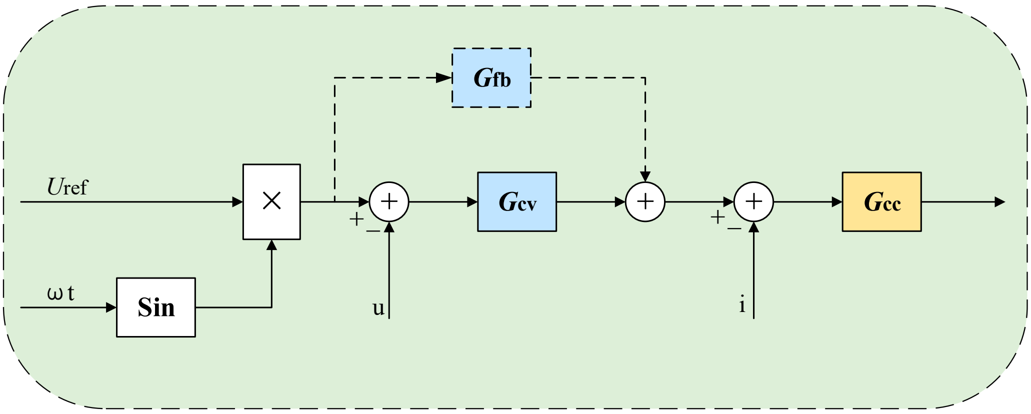

Figure 3. Control block diagram of the inverter module.

In Figure 3, the outer loop employed voltage loop control, where the reference voltage U_{ref} was subtracted from the output voltage and fed into the voltage loop, denoted G_{cv}. G_{fb} represents feedforward control. The output of the voltage loop G_{cv} was subtracted from the inverter output current and fed into the current loop G_{cc}, thus achieving dual closed-loop control of the voltage and current.

3. Control Strategy for the Inverter Module

In order to determine the optimal control strategy for the inverter module of the arc plasma power source, it was necessary to compare various control strategies and modulation methods. This comparison helped in selecting the most suitable control method for the aforementioned plasma power source inverter module.

3.1. Main Control Modes of the Inverter Module

The main control methods currently applied in inverters include PI control [35], PID control [36], PR control [37], and QPR control [38]. References [35–38] have achieved favorable control results by employing these inverter control methods based on various scenarios and systems. Table 2 compares the characteristics of these four control methods.

Table 2. Comparison of Characteristics of Main Control Methods.

Control Mode	Control Principle	Transfer Functions	Theoretical Control Effects
PI Control	According to the deviation between the given value and the actual output value, the proportion and the integral of the deviation were combined linearly to form a controlled quantity to control the object under control.	$G_{cv} = K_p + \frac{K_i}{s}$	Differential adjustment
PID Control	The addition of an extra differential link (D) to PI control enables better elimination of static errors, accelerates the control regulation process, reduces overshoot, and overcomes oscillations.	$G_{cv} = K_p + \frac{K_i}{s}$ $G_{fb} = \frac{1}{K_{fb}}$	Differential adjustment
PR Control	Proportional resonance controller, consisting of a proportional link and a resonance link, for static-free control of sinusoidal quantities.	$G_{cv} = K_p + \frac{2K_r s}{s^2+\omega^2}$	Non-differential adjustment
QPR Control	Quasi-proportional resonance controller, based on PR control, relieved the gain at the resonance point.	$G_{cv} = K_p + \frac{2K_r\omega_c s}{s^2+2\omega_c s+\omega^2}$	Non-differential adjustment

3.2. Main Modulation Methods of the Inverter Module

The common modulation methods are unipolar modulation and bipolar modulation. The waveform of bipolar modulation is positive and negative in half a cycle, while the waveform of unipolar modulation only changes within a unipolar range in half a cycle. It has the characteristics of low loss and small electromagnetic interference. Unipolar double-frequency modulation is the optimization of unipolar modulation. Although both output the same pulse, the carrier frequency is doubled in principle by unipolar double-frequency modulation. After the SPWM pulse sequence [39,40] passes through the driving module, different working modes of the four power transistors can be used. When using power devices with the same switching frequency, the voltage pulse frequency output by unipolar double-frequency modulation is twice that of unipolar modulation, which can reduce switching losses and improve the quality of the output voltage waveform. Therefore, this paper specifically focuses on comparing unipolar double-frequency modulation and bipolar modulation. Table 3 provides a detailed discussion of the differences between the two modulation methods.

Figure 4 shows the simulation model block diagram of the two modulation methods. Bipolar modulation compares the input voltage waveform with the carrier waveform (triangle waveform). When the amplitude of the modulating waveform exceeds that of the carrier waveform, switch tubes Q1 and Q4 produce high-level outputs, while Q2 and Q3 produce low-level outputs. On the other hand, if the amplitude of the modulating waveform is lower than that of the carrier waveform, Q2 and Q3 produce high-level outputs, while Q1 and Q4 produce low-level outputs. When the amplitudes of both modulating waveforms exceed the amplitude of the carrier waveform, Q1 and Q4 output a high level, while Q2 and Q3 output a low level. If the amplitude of one modulating waveform is low-er than that of the carrier waveform, either Q1 and Q4 or Q2 and Q3 will output a high level, but Q2 and Q4 cannot output a high level simultaneously.

Table 3. Comparison of Characteristics of the Two Modulation Methods.

Modulation Method	Modulation Principle	Advantages	Disadvantages
Bipolar modulation	When the modulating waveform amplitude is greater than the carrier waveform amplitude, switch tubes Q1 and Q4 are on and output high, Q2 and Q3 are off and output low, and vice versa.	Good common mode performance allows for higher output frequency response and reduces harmonic components.	Higher complexity, the need for more switching devices, and increases switching losses.
Monopole frequency doubling Modulation	The SPWM pulse sequence is obtained by modulating two sine waves with a half-switching period difference with a carrier triangle to control each of the two half-bridges in the full-bridge inverter, and the desired sinusoidal pulse sequence is obtained by precise control of the four power devices.	Lower switching losses, relatively simple control, and easier control of harmonic components in the output waveform [41].	Limited high-frequency response, and in complex applications, achieving sufficient control flexibility and precision may be challenging.

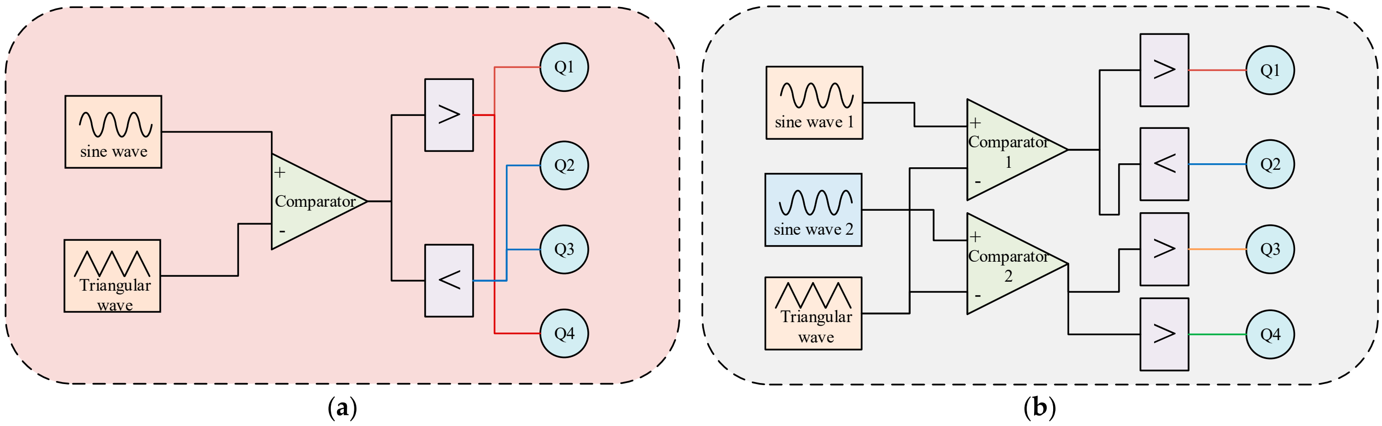

Figure 4. Modulation method simulation model block diagram: (**a**) bipolar modulation; (**b**) single-pole frequency modulation.

3.3. Simulation of the Inverter Module

To evaluate the strengths and weaknesses of the four control strategies (PI, PID, PR, and QPR) and two modulation methods (bipolar and unipolar frequency doubling), a simulation model based on the inverter module was developed on the MATLAB/Simulink simulation platform [42]. The simulation waveforms were observed, and their static-free tracking characteristics were compared, to determine the optimal method. The simulations were conducted at 50 Hz, and the waveforms were carefully analyzed to assess the performance of each strategy and modulation method. The relevant parameters of the simulation experiments are shown in Table 4.

Table 4. Parameters Related to Simulation Experiments.

Simulation Parameters	Set Values	Unit
DC-side voltage	400	V
Base voltage	311sinωt	V
Inverter switching frequency	50	Hz
Filter Inductors	1	mH
Filter capacitors	20	μF

According to the circuit structure diagram of the Inverter shown in Figure 2, the transfer function of the inverter could be derived using state equations [43]:

$$G(s) = \frac{R}{RLCs^2 + Ls + R} \tag{1}$$

Utilizing the Ziegler-Nichols critical gain method [44] for PI and PID parameter tuning, adjusting parameter values based on the Bode plots of PR and QPR to minimize steady-state error, achieved rapid system stabilization [45], and validated adjustments using the step response curve of the system transfer function $G(s)$. We identified the most suitable parameter values for all four control methods, ensuring that the step response curves exhibited excellent stability, overshot less than 20%, and response time was below 4 s [46].

Table 5 shows the control parameter settings for the four control methods, which are PI, PID, PR, and QPR in the simulation model [47].

Table 5. Setting Values for Control Parameters.

Control Methods	K_p	K_i	K_{fb}	K_r	ω_r	ω_c
PI control	0.01	10	/	/	/	/
PID control	0.01	10	500	/	/	/
PR control	0.02	1	/	1	100π	5π
QPR control	0.02	1	/	1	100π	5π

The modulation methods used in the simulation model were bipolar modulation and unipolar frequency doubling modulation. The control method employed a dual closed-loop control system, consisting of an external voltage loop and an internal current loop. There were four types of voltage loop control: PI control, PID control, PR control, and QPR control, and the current loop control was proportional. The block diagram of the arc plasma power inverter module simulation is shown in Figure 5.

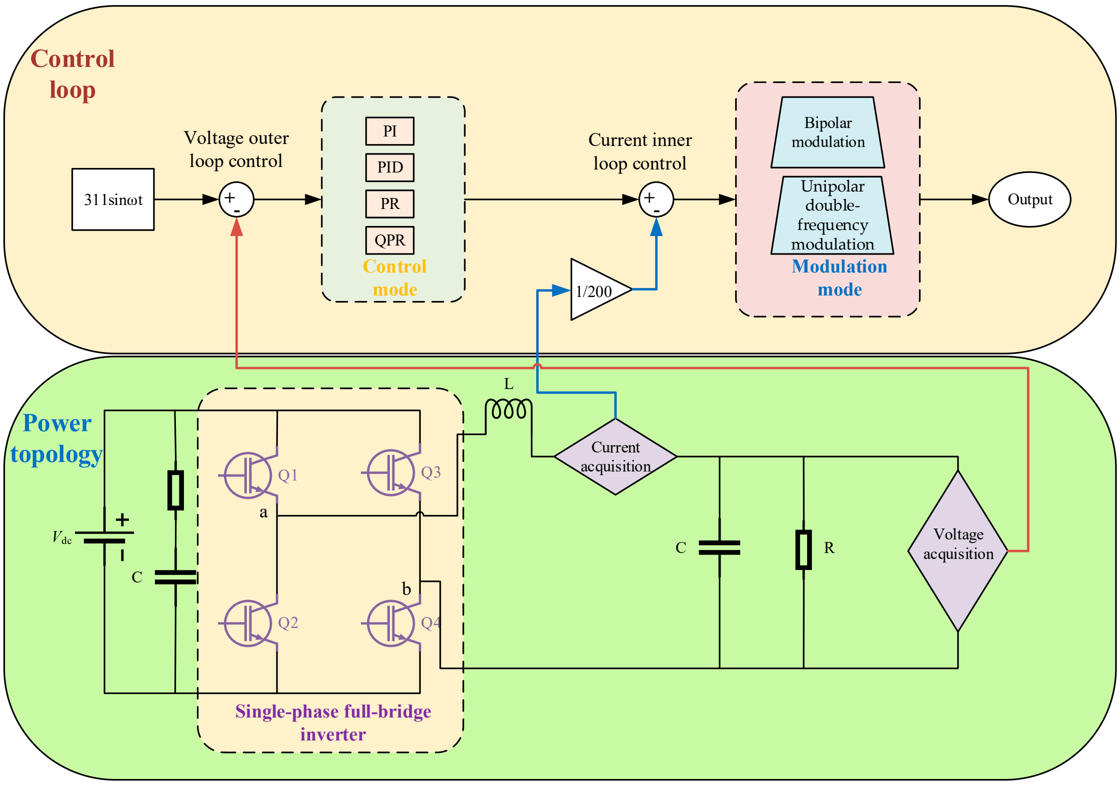

Figure 5. Block diagram of arc plasma power inverter module simulation.

The simulation model consisted of two main parts: the control loop and the power topology. In the control loop, V_0 was the output voltage, which was subtracted from the reference voltage and then passed through the voltage outer loop using one of the four control methods. The controlled output current was compared to the measured current, and the difference was subjected to SPWM modulation. To allow for a certain level of over-modulation, a limiting function was incorporated between the subtraction and the SPWM modulation. In the current loop control, the collected current was multiplied by a current loop coefficient and then subtracted to introduce some damping. This damping effect made the current regulation process smoother when there were variations in the load.

In the power topology, a constant current DC source was used with capacitors connected in parallel at both ends of the power supply to filter out spurious and AC components of the power supply. The power supply was then passed through the full-bridge inverter module in the arc plasma power simulation model, the LC filter, and finally connected to the load. During this process, the output voltage and current signals were collected.

4. Results and Analysis

4.1. Main Control Strategies of the Inverter Module

Figure 6 displays voltage simulation waveforms under single-polar carrier-based modulation for PI control, PID control, PR control, and QPR control, facilitating a comparative analysis of the waveform tracking performance across these four control methods. In the waveform plot under PI control, a certain phase difference existed between the grid voltage and the reference voltage, resulting in less-than-ideal tracking performance. PID control builds upon PI control by introducing feedforward control, reducing the burden of sinusoidal regulation by the PI controller. This enhanced the control of the sinusoidal waveform output. Although the tracking performance was improved compared to PI control, achieving zero steady-state tracking error remained unattained. Under PR control, nearly zero steady-state error regulation was achieved at the zero crossing point of the voltage. However, it was evident at the waveform resonance points that the difference between the output voltage and the reference voltage was still significant. In the waveform graph under QPR control, the phase difference between the output voltage and the reference voltage was essentially eliminated, and the waveforms closely matched. This achieved precise tracking without static errors, making it the optimal waveform tracking performance.

We used the Root Mean Square Error (*RMSE*) to measure the similarity between the output waveform and the reference waveform, thereby comparing the error between the output voltage waveform and the reference voltage waveform under different controls [48,49]. The definition of *RMSE* was given by the equation:

$$RMSE = \sqrt{\frac{1}{z}\sum_{i=0}^{z-1}(y_{0i} - y_{1i})^2} \tag{2}$$

Here, $y_{0\mathrm{i}}$ and $y_{1\mathrm{i}}$ represent the respective sampled values of the output voltage and the reference voltage waveforms, and z represents the total number of samples in the sinusoidal waveform. A smaller *RMSE* indicates a higher similarity between the output voltage waveform and the reference voltage waveform, resulting in better waveform tracking performance and improved waveform quality.

Upon calculation, the waveform zero crossing points, peak points, and overall *RMSE* values under the four control modes are presented in Table 6.

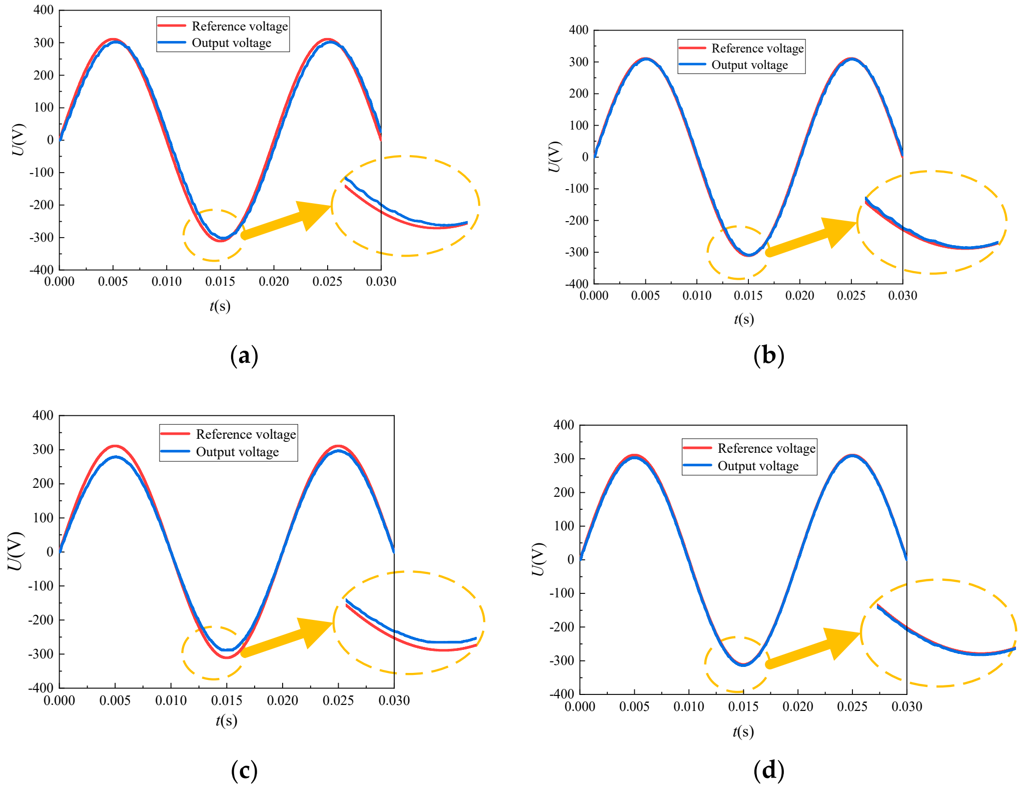

Figure 6. Voltage output waveforms under different control methods: (**a**) PI control; (**b**) PID control; (**c**) PR control; (**d**) QPR control.

Table 6. *RMSE* values under different control modes.

Control Method	*RMSE* at Zero Crossing Point (V)	*RMSE* at Peak Point (V)	Total *RMSE* (V)
PI	22.7927	12.3213	18.9213
PID	8.0795	4.0808	6.4401
PR	3.2038	19.8410	9.8194
QPR	4.9321	2.4780	2.6980

Based on the data presented in Table 6, it is evident that of the four control modes, QPR control demonstrated the most minimal steady-state error in the output voltage, signifying superior control performance.

The waveform distortion rate [50] was introduced to measure the magnitude of distortion occurring in the output voltage waveform. The total harmonic distortion rate (*THD*) of a voltage is the percentage of the square root of the sum of the squared RMS values of all the harmonics in that voltage waveform, excluding the fundamental, to the *RMS* value of the fundamental voltage of that waveform, i.e.:

$$THD = \frac{\sqrt{|V_2|^2 + |V_3|^2 + |V_4|^2 + |V_5|^2 + \ldots\ldots + |V_N|^2}}{|V_1|} \times 100\% = \sqrt{\sum_{n=2}^{N} \left(\frac{V_n}{V_1}\right)^2} \times 100\% \quad (3)$$

where: V_1 is the fundamental voltage component; V_2, V_3, V_4, V_5, …… V_{N} are integer multiples of the harmonic voltage components.

Utilizing Fast Fourier Transform (FFT) analysis [51,52], Figure 7 depicts the histogram of the distortion rate for each harmonic of the actual output voltage under unipolar octave modulation for the four control methods: PI control, PID control, PR control, and QPR control. It can be seen that the distortion rate of the second harmonic under PR control was large, but as the number of harmonics increased, the waveform distortion rate tended to decrease and the control effect gradually improved. At high harmonics, the harmonic distortion rates under PI and PID control were significantly higher than those under PR and QPR control.

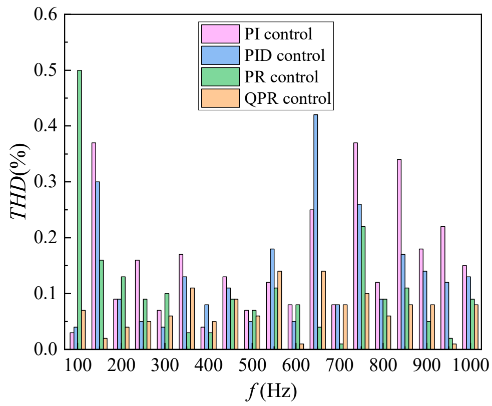

Figure 7. Distortion rate of each harmonic with different control methods.

Table 7 presents the total harmonic distortion rates for each control method. During system operation disturbances, the output voltage under PI control exhibited a total harmonic distortion rate of 0.71%, indicating a high level of harmonic content. Under PID control, the total harmonic distortion rate was reduced to 0.66%, a decrease of 0.05% compared to PI control, but still with significant harmonic content. PR control achieved a significantly lower total harmonic distortion rate of only 0.39%. Similarly, QPR control yielded a total harmonic distortion rate of 0.37%, approaching the performance of PR control and ensuring better voltage quality.

Table 7. Total Harmonic Distortion Rate Under Different Control Methods.

Control Method	THD
PI control	0.71%
PID control	0.66%
PR control	0.39%
QPR control	0.37%

Through adjustments to operating conditions, involving variations in the DC-side voltage (U_{dc}) and inverter switching frequency, a comparative assessment of the four control methods was conducted. Initially, with the inverter switching frequency held constant, modifications were made to the magnitude of the DC-side voltage (U_{dc}). The resulting variations in the *THD* of the output voltage are illustrated in Figure 8.

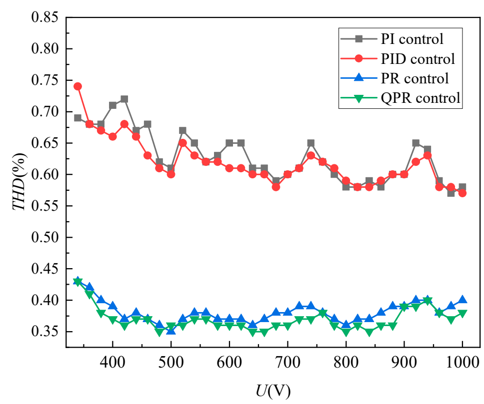

Figure 8. Effect of different input voltages on the total harmonic distortion rate of the output voltage.

As can be seen from Figure 8, the total harmonic distortion rate of the output voltage under PR control and QPR control was smaller than that under PI control and PID control. As the voltage on the DC side increased, the total harmonic distortion rate of the output voltage decreased under PI control and PID control, resulting in improved control effectiveness. On the other hand, the performance of PR control and QPR control remained relatively consistent, but still better than that of PI control and PID control. Consequently, as the voltage on the DC side increased, the control effectiveness can be ranked as follows: QPR control > PR control > PID control > PI control.

Furthermore, keeping the input voltage constant and varying the inverter switching frequency f, the change in the total harmonic distortion rate of the output voltage was obtained, as shown in Figure 9.

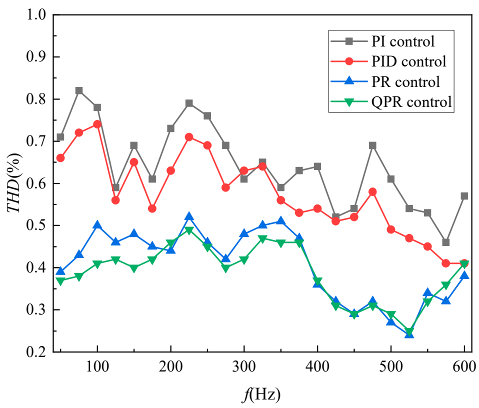

(**a**)

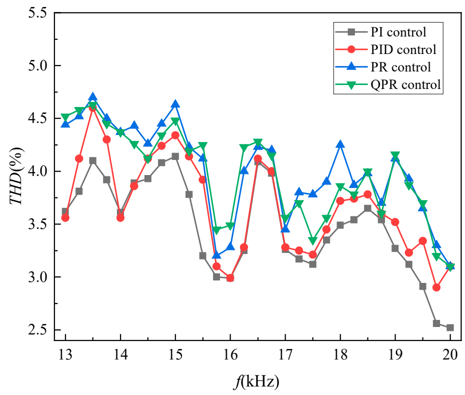

(**b**)

Figure 9. Effect of different frequencies on the total harmonic distortion rate of the output voltage: (**a**) Low frequency; (**b**) High frequency.

Modifying the magnitude of the inverter switching frequency caused a more pronounced impact on the total harmonic distortion rate of the output voltage. At lower frequencies, the total harmonic distortion rate of the output voltage under PR control and QPR control was lower than that under PI control and PID control. At higher frequencies, the total harmonic distortion rate of the output voltage under PR and QPR control was higher than that under PI and PID control. It is apparent that the magnitude of the inverter switching frequency had a significant impact on the effectiveness of the four control methods. In high-frequency scenarios, the total harmonic distortion rate of the output voltage under QPR control was minimized, measuring below 4.2%. Conversely, in low-frequency situations, the total harmonic distortion rate under PI control was also minimized, falling below 0.47%. Compared to previous research [29–31], the dual closed-loop control strategy with a voltage outer loop and a current inner loop used in this paper resulted in a lower distortion rate in the output voltage waveform, and it strictly conformed to the IEEE 519 standard [53] under all operating conditions.

At lower frequencies, PR control and QPR control exhibited superior performance compared to PI control and PID control. Figure 10 illustrates the Bode diagram for PR control and QPR control, different color lines represent the amplitude gain and phase angle of the two control methods at their respective frequencies. As the switching frequency increased, the gain of both PR and QPR control gradually decreased, resulting in a narrower bandwidth. Consequently, the control effectiveness diminished, and the stability of the system was compromised. Although PR control provided high gain at the resonant point, its bandwidth was narrower, resulting in less effective control compared to QPR control. Therefore, at lower frequencies, QPR control yields the best performance.

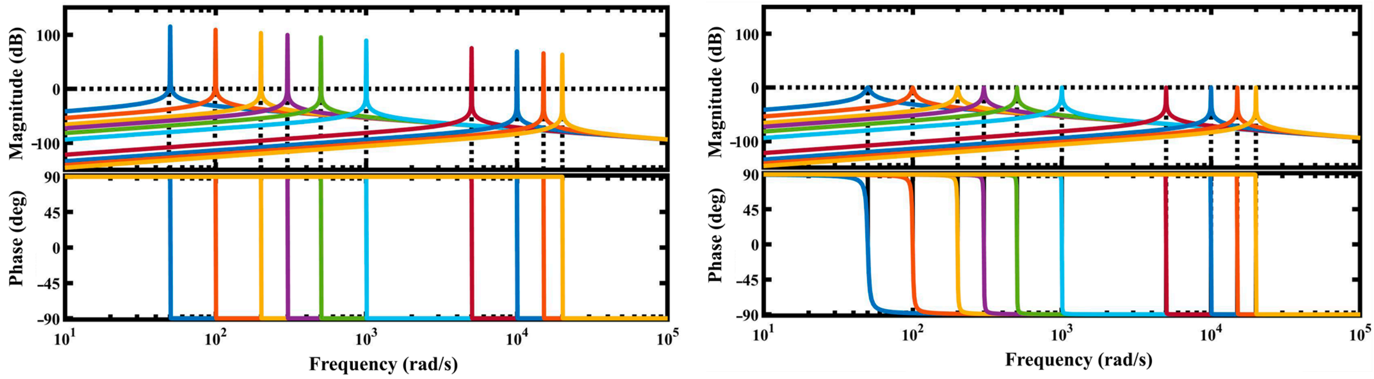

(**a**) (**b**)

Figure 10. Porter diagram for different control methods with varying ω: (**a**) PR control; (**b**) QPR control.

When operating at high frequencies, PI control and PID control outperformed PR control and QPR control. PID control, in contrast to PI control, introduced a phase lead compensation. When dealing with high-frequency situations characterized by rapid responses, system overshooting could occur, and the integrator could accumulate errors to accommodate this overshooting. Enhancing the integral action appropriately could lead to improved control performance. However, incorporating a differential component may result in high-frequency oscillations that degrade control performance [54]. Consequently, when the switching frequency is high, PI control delivered optimal results.

4.2. Influence of the Control Method

Under the QPR control method, the total harmonic distortion rate was 0.37% after Fast Fourier Transform analysis, while the total harmonic distortion rate under the bipolar modulation method was 0.53%, 0.15% higher than that of the unipolar frequency doubling. This indicated that unipolar frequency doubling modulation had a better modulation effect and the modulated waveform was closer to the ideal sine.

Figure 11 shows the variation in the total harmonic distortion rate of the output voltage when modifying the input voltage U_{dc} and the inverter switching frequency f on the DC side.

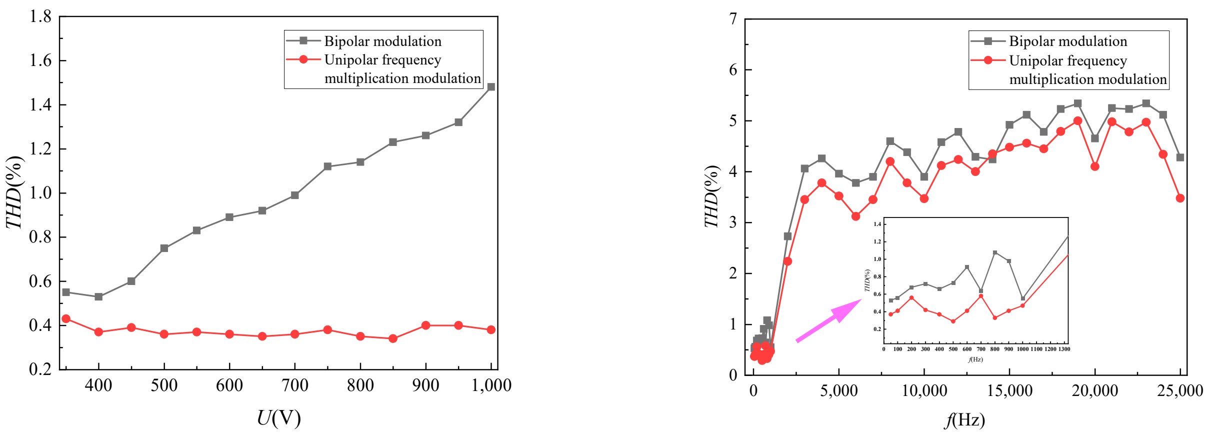

(**a**) (**b**)

Figure 11. Plot of total harmonic distortion of output voltage with voltage and frequency: (**a**) Voltage change; (**b**) Frequency change.

Figure 11 reveals that as the voltage increased, the distortion in the waveform became more pronounced under bipolar modulation. In contrast, the *THD* of the output waveform under unipolar double-frequency modulation was relatively stable, with excellent modulation performance, consistently remaining below 0.47%. As the switching frequency increased, although both bipolar modulation and unipolar double-frequency modulation exhibited degraded performance, the *THD* of the output voltage under unipolar double-frequency modulation consistently remained below 4.2%, achieving a high level of modulation performance. Therefore, regardless of the operating conditions, unipolar double-frequency modulation consistently yielded the best results.

5. Conclusions

This paper focuses on the inverter module of arc plasma power sources. In its design, it utilized a dual closed-loop control structure with a voltage outer loop and a current inner loop. In terms of control, building upon prior research, it varied the operating conditions and undertook a comparative study of the advantages and disadvantages of different control methods and modulation techniques. Furthermore, a simulation model was constructed using Matlab/Simulink. This model was employed to conduct a quantitative analysis and a comparative examination, utilizing waveform tracking performance, voltage waveform distortion rate, and steady-state error as evaluation metrics. The primary objective was to pinpoint the most effective control strategy, thereby mitigating the pollution resulting from harmonics, enhancing the power quality of the inverter module, and ultimately elevating the stability of the arc plasma power source system.

Based on the test results, operating at lower frequencies, within the range of 0 to 1 kHz for the switching frequency of the arc plasma power source, the control strategy that combined QPR control with single-pole harmonic modulation delivered the most effective voltage waveform tracking performance. It resulted in a distortion rate of less than 0.47% and the lowest steady-state error. On the other hand, at higher switching frequencies, when the switching frequency of the arc plasma power source exceeded 1 kHz, utilizing the control strategy of PI control with single-pole harmonic modulation provided the best voltage waveform tracking performance, with a distortion rate below 4.2% and minimal steady-state error. Applying these two control strategies to different operating conditions enabled seamless tracking of sinusoidal signals without any steady-state error. This effectively reduced voltage harmonics, leading to excellent voltage quality, enhanced system resilience, and strict compliance with the IEEE 519 standard. It can offer valuable theoretical support and practical guidance for future engineering applications related to inverters.

Author Contributions: Conceptualization, H.Y. and Y.J.; methodology, Y.L., C.J. and Y.J.; software, Y.L., C.J. and Y.J.; validation, Y.L. and Y.J.; formal analysis, Y.L., C.J. and Y.J.; investigation, Y.L. and Y.J.; resources, Y.L., C.J. and Y.J.; data curation, Y.L., H.Y. and Y.J.; writing—original draft preparation, Y.L., C.J., and Y.J.; writing—review and editing, Y.L. and Y.J.; visualization, Y.L. and Y.J.; supervision, H.Y. and Y.J.; project administration, H.Y., C.J. and Y.J.; funding acquisition, Y.L. and H.Y. All authors have read and agreed to the published version of the manuscript.

Funding: This work was funded by the Postgraduate Research & Practice Innovation Program of Jiang Province under Grant SJCX22_1438.

Data Availability Statement: The authors confirm that the data supporting the findings of this study are available within the article.

Conflicts of Interest: The authors declared that they do not have any commercial or associative interest that represents a conflict of interest in connection with the work submitted.

References

1. Li, J.; Liu, K.; Yan, S.; Li, Y.; Han, D. Application of thermal plasma technology for the treatment of solid wastes in China. *Waste Manag.* **2016**, *58*, 260–269. [CrossRef] [PubMed]
2. Bhatt, K.P.; Patel, S.; Upadhyay, D.S.; Patel, R.N. A critical review on solid waste treatment using plasma pyrolysis technology. *Chem. Eng. Process.* **2022**, *177*, 108989. [CrossRef]
3. Dovilė, G.; Mindaugas, A.; Andrius, T. *Recent Advances in Renewable Energy Technologies*; Academic Press: Cambridge, MA, USA, 2022; Chapter 4.

4. Zhou, F.; Ma, H.D.; Chen, H.; Zhu, X.; Liu, X. Research progress of AC arc plasma torch and its application. *J. Aerodyn.* **2022**, *40*, 15–29. [CrossRef]
5. Zhou, G.; Xu, J. A Comprehensive Review of Switching Converter Modulation and Control Techniques. *Chin. J. Electr. Eng.* **2014**, *34*, 815–831.
6. Mattavelli, P. An improved deadbeat control for UPS using disturbance observers. *IEEE Trans. Ind. Electron.* **2005**, *52*, 206–212. [CrossRef]
7. Blaabjerg, F.; Teodorescu, R.; Liserre, M.; Timbus, A.V. Overview of control and grid synchronization for distributed power generation systems. *IEEE Trans. Ind. Electron.* **2006**, *53*, 1398–1409. [CrossRef]
8. Cortes, P.; Ortiz, G.; Yuz, J.I.; Rodriguez, J.; Vazquez, S.; Franquelo, L.G. Model predictive control of an inverter with output LC filter for UPS applications. *IEEE Trans. Ind. Electron.* **2009**, *56*, 1875–1883. [CrossRef]
9. Deng, H.; Oruganti, R.; Srinivasan, D. Analysis and design of iterative learning control strategies for ups inverters. *IEEE Trans. Ind. Electron.* **2007**, *54*, 1739–1751. [CrossRef]
10. Tai, T.-L.; Chen, J.-S. UPS inverter design using discrete-time sliding-mode control scheme. *IEEE Trans. Ind. Electron.* **2002**, *49*, 67–75. [CrossRef]
11. Hu, J.; Shang, L.; He, Y.; Zhu, Z. Direct active and reactive power regulation of grid-connected DC/AC converters using sliding mode control approach. *IEEE Trans. Power Electron.* **2010**, *26*, 210–222. [CrossRef]
12. Benyoucef, A.; Kara, K.; Chouder, A.; Silvestre, S. Prediction-based deadbeat control for grid-connected inverter with L-filter and LCL-filter. *Electr. Power Compon. Syst.* **2014**, *42*, 1266–1277. [CrossRef]
13. Parvez, M.; Elias, M.; Rahim, N.; Osman, N. Current control techniques for three-phase grid interconnection of renewable power generation systems: A review. *Sol. Energy* **2016**, *135*, 29–42. [CrossRef]
14. Kennel, R.M.; Kazmierkowski, M.; Rodriguez, J.; Cortes, P. Predictive control in power electronics and drives. *IEEE Int. Symp. Ind. Electron.* **2008**, *55*, 4312–4324. [CrossRef]
15. Gálvez-Carrillo, M.; De Keyser, R.; Ionescu, C. Nonlinear predictive control with dead-time compensator: Application to a solar power plant. *Sol. Energy* **2009**, *83*, 743–752. [CrossRef]
16. Yan, W.; Hu, J.; Utkin, V.; Xu, L. Sliding mode pulse width modulation. *IEEE Trans. Power Electron.* **2008**, *23*, 619–626. [CrossRef]
17. Schirone, L.; Celani, F.; Macellari, M. Discrete-time control for DC-AC converters based on sliding mode design. *IET Power Electron.* **2012**, *5*, 833–840. [CrossRef]
18. Navarro-López, E.M.; Cortés, D.; Castro, C. Design of practical sliding-mode controllers with constant switching frequency for power converters. *Electr. Power Syst. Res.* **2009**, *7*, 796–802. [CrossRef]
19. Wai, R.-J.; Wang, W.-H. Grid-connected photovoltaic generation system. *IEEE Trans. Circuits Syst.* **2008**, *55*, 953–964. [CrossRef]
20. Tan, S.-C.; Lai, Y.; Chi, K.T. Indirect sliding mode control of power converters via double integral sliding surface. *IEEE Trans. Power Electron.* **2008**, *23*, 600–611. [CrossRef]
21. Aamir, M.; Kalwar, K.A.; Mekhilef, S. Proportional-resonant and slide mode control for single-phase UPS inverter. *Electr. Power Compon.* **2017**, *45*, 11–21. [CrossRef]
22. Abrishamifar, A.; Ahmad, A.; Mohamadian, M. Fixed switching frequency sliding mode control for single-phase unipolar inverters. *IEEE Trans. Power Electron.* **2012**, *27*, 2507–2514. [CrossRef]
23. Carpita, M.; Marchesoni, M. Experimental study of a power conditioning system using sliding mode control. *IEEE Trans. Power Electron.* **1996**, *11*, 731–742. [CrossRef]
24. Chiang, S.; Tai, T.; Lee, T. Variable structure control of UPS inverters. *IEE Proc. Electr. Power Appl.* **1998**, *145*, 559–567. [CrossRef]
25. Kukrer, O.; Komurcugil, H.; Doganalp, A. A three-level hysteresis function approach to the sliding-mode control of single-phase UPS inverters. *IEEE Trans. Ind. Electron.* **2009**, *56*, 3477–3486. [CrossRef]
26. Gu, D.; Yao, Y.; Zhang, D.M.; Cui, Y.B.; Zeng, F.Q. Matlab/Simulink Based Modeling and Simulation of Fuzzy PI Control for PMSM. *Procedia Comput. Sci.* **2020**, *166*, 195–199. [CrossRef]
27. Zammit, D.; Staines, C.S.; Apap, M.; Licari, J. Design of PR current control with selective harmonic compensators using Matlab. *J. Electr. Syst. Inf. Technol.* **2017**, *4*, 347–358. [CrossRef]
28. Yang, L.; Ye, M.; Wang, Y.; Xu, Q.; Meng, X. A novel low frequency current ripple suppression method for energy storage system in DC microgrid. *Electric. Power. Syst. Res.* **2022**, *213*, 108748. [CrossRef]
29. Parvez, M.; Elias, M.F.M.; Rahim, N.A.; Blaabjerg, F.; Abbott, D.; Al-Sarawi, S.F. Comparative Study of Discrete PI and PR Controls for Single-Phase UPS Inverter. *IEEE Access* **2020**, *8*, 45584–45595. [CrossRef]
30. Li, J.; Xu, S.; Hui, D. A Study on a Suitable PI and Quasi-PR Control Strategy for Energy Storage PCS. *New Technol. Electr. Eng. Energy* **2016**, *35*, 54–61. [CrossRef]
31. Wang, X.; Mao, R.; Tian, B.; Huang, Q. Current Optimization of Photovoltaic Grid Integration Based on PI and Quasi-PR Joint Control. *Power Syst. Prot. Control* **2017**, *45*, 121–125. [CrossRef]
32. Monirul, I.; Saad, M.; Mahamudul, H. Single phase transformerless inverter topologies for grid-tied photovoltaic system. *Renew. Sustain. Energy Rev.* **2015**, *45*, 69–86. [CrossRef]
33. Yuan, L.; Xiu, C.; Ma, X. Sliding mode control strategy for microgrid inverter systems. *Power Electron.* **2023**, *23*, 821–831. [CrossRef]
34. Huang, R.H.; Xie, S.J. Double-loop digital control strategy based on proportional-resonant controller. *Trans. China Electrotech. Soc.* **2012**, *27*, 77–81.

35. Qian, N.S. Simulation Study of Single-Phase Photovoltaic Grid-Connected Inverter Based on PI Control. *Guangdong Electr. Power* **2012**, *25*, 57–60. [CrossRef]
36. Jin, Y.Y.; Wang, Z.S.; Chen, H.M.; Liu, H. Design of Single-Phase Inverter PID Controller Based on Root Locus. *Electromechanical Eng.* **2008**, *25*, 83–85. [CrossRef]
37. Wang, Y.S.; Wang, S.Y.; Hai, R. Harmonic Suppression Strategy of Grid-Connected Inverter Based on PR Regulator. *Power Supply Technol.* **2016**, *40*, 184–188. [CrossRef]
38. Liu, Y.X.; Teng, Q.F. Control Research of Grid-Connected Inverter Based on QPR Regulator for Harmonic Compensation. *J. Lanzhou Jiaotong Univ.* **2020**, *39*, 67–74. [CrossRef]
39. Yaşar, B.; Kaner, Y.; Volkan, K. Design of a single-phase SPWM inverter application with PIC micro controller. *Eng. Sci. Technol.* **2019**, *22*, 592–599. [CrossRef]
40. Wang, W.; Li, K.; Liu, Z.Y. Research on frequency doubling technology and harmonic suppression method of SPWM inverter. *Micromotors* **2015**, *6*, 60–64. [CrossRef]
41. Zhang, G.R.; Yan, L.H. Research on Transmission Bandwidth of Unipolar Carrier-Based CPS-SPWM. *Power Syst. Prot. Control* **2018**, *46*, 1–8. [CrossRef]
42. Sang, H.K. Pulse width modulation inverters. *Electr. Mot. Control* **2017**, *7*, 265–340. [CrossRef]
43. Du, G.; Zhang, P.; Luo, R.J.; LI, H. Research on Dual-Closed-Loop SPWM Inverter Control Strategy Based on Particle Swarm Optimization. *Electron. Devices* **2020**, *43*, 815–819. [CrossRef]
44. Vladimír, B.; Jinří, M.; Roman, P. Tuning of Digital PID Controllers Based on Ziegler—Nichols Method. *IFAC Proc.* **1997**, *30*, 145–150. [CrossRef]
45. Song, S.J.; Yang, X.; Liu, B.; Liao, B.; Song, C. Grid-Connected Inverter Quasi-Proportional Resonant Control Based on Grid Impedance. *China Electr. Power* **2019**, *52*, 90–96.
46. Liu, Y.Z. *Design of Overshoot-Free PID Controller*; Hangzhou Dianzi University: Hangzhou, China, 2010; Volume 4, pp. 25–42. [CrossRef]
47. Huang, X.L.; Feng, X.D.; Zhang, X.X. Influence of QPR controller parameters on the adaptability of weak power grid of converter. *Electr. Drive* **2020**, *50*, 28–34. [CrossRef]
48. Liu, E.; Han, Y.; Zalhaf, A.S.; Yang, P.; Wang, C. Performance evaluation of isolated three-phase voltage source inverter with LC filter adopting different MPC methods under various types of load. *Control Eng. Pract.* **2023**, *135*, 105520. [CrossRef]
49. Ćalasan, M.; Aleem, S.H.A.; Zobaa, A.F. On the root mean square error (RMSE) calculation for parameter estimation of photovoltaic models: A novel exact analytical solution based on Lambert W function. *Energy Convers. Manag.* **2020**, *210*, 112716. [CrossRef]
50. Fu, W.P.; Wang, X.H.; Wang, H. Analysis of power supply voltage waveform distortion rate. *J. Chang. Electr. Power Inst.* **2001**, *16*, 47–49. [CrossRef]
51. Fu, J.M. Harmonic analysis of single-phase SPWM inverter circuit based on MATLAB. *Sci. Technol. Innov.* **2021**, *21*, 24–26. [CrossRef]
52. Ye, Q.; Ruan, Y.; Ma, Z. Simulation analysis of total harmonic distortion rate of voltage in inverter circuit. *Proc. Chin. Soc. Electr. Power Syst. Autom.* **2010**, *22*, 100–102. [CrossRef]
53. Lin, H. Introduction to Current Limits in the American Harmonic Standard IEEE Std. 519. *Power Supply* **2012**, *29*, 11–14. [CrossRef]
54. Han, Y.F.; Shen, H.F.; He, G.F.; Fan, X.H.; Zhao, Q.Y. Application of composite proportional resonance control in multi-inverter grid-connected system. *Meas. Control Technol.* **2018**, *37*, 122–127. [CrossRef]